

Geminga SNR: Possible candidate of local cosmic-ray factory

BING ZHAO,¹ WEI LIU,² QIANG YUAN,^{3,4,5} HONG-BO HU,^{2,6} XIAO-JUN BI,^{2,6} HAN-RONG WU,² XUN-XIU ZHOU,¹ AND
YI-QING GUO^{2,6}

¹*Southwest Jiaotong University, 610031 Chengdu, Sichuan, China*

²*Key Laboratory of Particle Astrophysics, Institute of High Energy Physics, Chinese Academy of Sciences, Beijing 100049, China*

³*Key Laboratory of Dark Matter and Space Astronomy, Purple Mountain Observatory, Chinese Academy of Sciences, Nanjing 210008, China*

⁴*School of Astronomy and Space Science, University of Science and Technology of China, Hefei 230026, China*

⁵*Center for High Energy Physics, Peking University, Beijing 100871, China*

⁶*University of Chinese Academy of Sciences, Beijing 100049, China*

ABSTRACT

The precise measurements of energy spectra and anisotropy could help us uncover the local cosmic-ray accelerators. Our recent works have shown that spectral hardening above 200 GeV in the energy spectra and transition of large-scale anisotropy at ~ 100 TeV are of local source origin. Less than 100 TeV, both spectral hardening and anisotropy explicitly indicate the dominant contribution from nearby sources. In this work, we further investigate the parameter space of sources allowed by the observational energy spectra and anisotropy amplitude. To obtain the best-fit source parameters, a numerical package to compute the parameter posterior distributions based on Bayesian inference, which is applied to perform an elaborate scan of parameter space. We find that by combining the energy spectra and anisotropy data, the permissible range of location and age of local source is considerably reduced. When comparing with the current local SNR catalog, only Geminga SNR could be the proper candidate of the local cosmic-ray source.

1. INTRODUCTION

As far back as 1930s, the supernova remnants (SNRs) had been proposed as the sources of Galactic cosmic rays (CRs) (Baade & Zwicky 1934). However due to the diffusive character of CR propagation in the Galaxy, it is hardly to locate their acceleration sites by tracing back the arrival directions of CRs, with a possible exception of ultra-high energy CRs. What have been achieved in identifying CR sources up to now are mostly indirect, namely through the multi-wavelength observations of electromagnetic emission from SNRs, see the reference of (Cardillo et al. 2014; Funk 2015; Dubner & Giacani 2015; Hewitt & Lemoine-Goumard 2015). On the other hand, Mertsch (2011); Bernard et al. (2012) have shown that CRs from the nearby young sources, within 1 – 2 kpc from the solar system, could give rise to large fluctuations of observed energy spectrum. As a result, the unexpected observational features probably relate to these local sources. Meanwhile within this short distance, the CR sources are finite and discrete, thus they

are easier to be found by the multi-wavelength observations. Therefore it is promising to directly unveil the local CR accelerators by relating the observational features of CRs to the local source.

In fact, the single source model, in which one or a few nearby young sources make nonnegligible contribution to the spectrum, was initially put forward for the purpose of the sharpness of the knee region at $\sim 3 - 4$ PeV in the all-particle spectrum (Erlykin & Wolfendale 1997). Later with more and more advanced instruments being put into use, the measuring accuracy has been promoted greatly and more novel features in the energy spectrum are uncovered. The single source model and its extension - local source model, are widely used to interpret various observational phenomena. Usually, the propagation of CRs from the nearby source is time-dependent, and the propagated spectrum resembles a bump-like structure, which is deemed as an excess of CR flux. Thus the local pulsar or SNR could be the naturally origin of the positron excess above 10 GeV (Adriani et al. 2009; Abdo et al. 2009; Accardo et al. 2014; Aguilar et al. 2014) and spectral hardening of nuclei above 200 GeV (Panov et al. 2007, 2009; Yoon et al. 2011; Adriani et al. 2011; Aguilar et al. 2015b,a; Adriani

et al. 2019) and ensuing softening at ~ 20 TeV (Yoon et al. 2017; Atkin et al. 2017; An et al. 2019). Meanwhile it could also account for the break in all-electron spectrum at TeV energies (Aharonian et al. 2009; Borla Tridon 2011; Staszak et al. 2015; DAMPE Collaboration et al. 2017). Furthermore, in the traditional propagation model, the predicted anisotropy amplitude from background SNRs far exceeds the measurements, which is only about $10^{-4} - 10^{-3}$ (Blasi & Amato 2012). The local source could effectively lower the amplitude, if it lies close to the direction of anti-Galactic center (Ahlers 2016; Liu et al. 2017).

In recent works, we established a coherent picture to explain both observed spectral features and anisotropy (Liu et al. 2019; Qiao et al. 2019). We find that the amplitude transition and phase flipping in the dipole anisotropy map have a common origin with the spectral hardening of nuclei above 200 GeV and ensuing falloff at ~ 20 TeV. Less than 100 TeV, the anisotropy and spectral features are dominated by the local source. The position of local source is close to the direction of anti-Galactic center and far from the Galactic disk. We find that the Geminga SNR at its pulsar's birth place could be a prime candidate.

In fact, Geminga pulsar has long been considered as a local positron source, since the discovery of the increasing positron fraction above 10 GeV. Recently HAWC experiment measured the extended TeV gamma-ray emission of Geminga and PSR B0656+14 pulsars (Abeysekara et al. 2017). The inferred diffusion coefficient nearby the γ -ray emission region is far less than the standard value derived by fitting the B/C ratio. It suggested the positron excess may have an exotic origin. However Fang et al. (2018) and Tang & Piran (2019) argued that even the inference in view of the HAWC surface brightness profile is correct, the positron excess could still be accounted for by the Geminga pulsar, as long as introducing a two-zone diffusion model.

In this work, we aim at the parameter space of cosmic-ray sources permitted by the observed energy spectra and anisotropy. To perform the elaborate scan of parameter space of sources, the multinest package, based on Bayesian inference, is applied. By fitting the energy spectra and anisotropy amplitude, the permissible space of location and age of local source is greatly reduced. Our study further demonstrates that the Geminga SNR could be the best candidate of local cosmic-ray source.

The rest paper is organized as follows: In Sec.2, the propagation model and Bayesian inference are briefly introduced. Sec.3 presents the calculated results and Sec.4 is reserved for the conclusion.

2. MODEL DESCRIPTION

2.1. Propagation Model

The spatial-dependent propagation (SDP) model has received a lot of attention in recent years. It was first introduced as a Two Halo model (THM) (Tomassetti 2012) to explain the spectral hardening of both proton and helium above 200 GeV (Adriani et al. 2011). Afterwards, it is further applied to secondary and heavier components (Tomassetti 2015; Feng et al. 2016; Guo et al. 2016; Liu et al. 2018; Tian et al. 2020; Yuan et al. 2020), diffuse gamma-ray distribution (Guo & Yuan 2018) and large-scale anisotropy (Liu et al. 2019; Qiao et al. 2019). For a comprehensive introduction, one can refer to Guo et al. (2016) and Liu et al. (2018).

In the SDP model, the whole diffusive halo is divided into two parts. The Galactic disk and its surrounding area are called the inner halo (IH) region, in which the diffusion coefficient is spatial dependent and relevant to the radial distribution of background CR sources. The extensive diffusive region outside the IH is named as the outer halo (OH) region, where the diffusion is regarded as only rigidity dependent. The size of IH is represented by its half thickness ξ_{zh} , whereas the OH region's is $(1 - \xi)z_h$. The diffusion coefficient D_{xx} in the diffusive halo is thus parameterized as:

$$D_{xx}(r, z, \mathcal{R}) = D_0 F(r, z) \beta^\eta \left(\frac{\mathcal{R}}{\mathcal{R}_0} \right)^{\delta_0 F(r, z)} \quad (1)$$

where

$$F(r, z) = \begin{cases} g(r, z) + [1 - g(r, z)] \left(\frac{z}{\xi z_0} \right)^n, & |z| \leq \xi z_0 \\ 1, & |z| > \xi z_0 \end{cases} \quad (2)$$

with $g(r, z) = N_m / [1 + f(r, z)]$. $f(r, z)$ is the source density distribution, which is approximated as axisymmetric, i.e. $f(r, z) = \left(\frac{r}{r_\odot} \right)^\alpha \exp \left[-\frac{\beta(r - r_\odot)}{r_\odot} \right] \exp \left(-\frac{|z|}{z_s} \right)$ with $r_\odot \equiv 8.5$ kpc and $z_s = 0.1$ kpc. The parameters α and β are taken as 1.09 and 3.87 respectively in this work (Green 2015). The propagation of CRs from local point source is time-dependent. As for the instantaneous injection, the spatial distribution is $\psi(\mathcal{R}, \mathbf{r}, t) = Q(\mathcal{R}) e^{-(\mathbf{r} - \mathbf{r}')^2 / (4D_{xx}t)} / (4\pi D_{xx}t)^{3/2}$. The energy spectra at sources are assumed to have a power-law of rigidity plus an exponential cutoff,

$$q(\mathcal{R}) \propto \mathcal{R}^{-\nu} \exp \left(-\frac{\mathcal{R}}{\mathcal{R}_c} \right) \quad (3)$$

In this work, the diffusion-reacceleration (DR) propagation model is adopted. The numerical package

DRAGON (Evoli et al. 2008) is used to solve the diffusion equation to obtain the CR distribution. Less than tens of GeV, the CR fluxes are impacted by solar wind. The force-field approximation is applied to describe the solar modulation effect (Gleeson & Axford 1968; Perko 1987).

2.2. Bayesian Parameter Inference

Bayesian analysis method has now been widely used in astrophysics, cosmology as well as particle physics for the parameter inference. In this work, to quantitatively evaluate the probability density distribution (PDF) of model parameters permitted by the observed CR spectra and anisotropy amplitude, the Bayesian inference approach is applied. Here we give a brief introduction to the Bayesian inference of parameters. For a more comprehensive review, one can refer to Trotta (2008); Putze et al. (2009); Trotta et al. (2011); Feng et al. (2016).

Bayesian inference is essentially to make use of prior PDF for the parameters of interest and the likelihood function supplied by the data to evaluate the posterior PDFs. Given the parameter set Θ and the observational data D , Bayes Theorem reads

$$P(\Theta|D) = \frac{P(D|\Theta)P(\Theta)}{P(D)}. \quad (4)$$

$P(\Theta|D)$ is the posterior PDF of the parameters, while $P(\Theta)$ is the prior PDF of parameters before the observations are considered. $P(D|\Theta) = L(\Theta)$ is called the likelihood function, a function of Θ given the data set D . The likelihood function is defined as

$$\mathcal{L}(\Theta) = \exp\left(-\frac{1}{2}\chi^2(\Theta)\right), \quad (5)$$

with $\chi^2(\Theta)$ built from the data and model, i.e.

$$\chi^2(\Theta) = \sum_{i=1}^{N_{\text{data}}} \left(\frac{y_i^{\text{exp}} - y_i^{\text{th}}(\Theta)}{\sigma_i} \right)^2, \quad (6)$$

in which y_i^{exp} and σ_i are the measured value and standard deviation in experiment, and y_i^{th} is the theoretical expectation under certain parameter set Θ . The denominator in Eq. (4), named the Bayesian evidence, is obtained by computing the average of the likelihood under the prior, i.e.

$$P(D) = \int P(D|\Theta)P(\Theta)d\Theta. \quad (7)$$

In the parameter estimation, the inferences are obtained by taking samples from the posterior using MCMC sampling methods, where at equilibrium the chain contains a set of samples from the parameter

space distributed according to the posterior. With the posterior samples, the marginal posterior PDFs and other estimations could be available straightforward.

In this work, we adopt the public MultiNest package (Feroz & Hobson 2008; Feroz et al. 2009, 2019), which implements the nested sampling algorithm (Skilling 2004). Compared with the traditional Markov chain Monte Carlo (MCMC) methods, the nested sampling could navigate the parameter space with complex, multimodal posterior distribution until a well-defined termination point with high efficiency.

3. RESULTS

The propagation and injection parameters are evaluated independently and the former can be determined by fitting B/C and $^{10}\text{Be}/^9\text{Be}$ ratios. As for the SDP model, the unknown propagation parameters are D_0 , δ_0 , Nm , ξ , n , v_A and z_h respectively. Fig. 1 shows the comparison of the B/C and $^{10}\text{Be}/^9\text{Be}$ ratios between the SDP predictions and the data. The values of corresponding propagation parameters are listed in table 1. The red lines is the B/C ratio computed only from background sources, and the black line is the one with additional carbon contribution from local source. As can be seen that, the carbon flux from the local source lowers the total B/C ratio above ~ 10 GeV. Within the uncertainty of the measurements, the computed B/C ratio is still consistent with the latest AMS-02 measurement. Due to lack of the precise observation, the measurements of $^{10}\text{Be}/^9\text{Be}$ have large errors, and our fitting could also account for the current data.

Tab. 1. Fitted spatial-dependent propagation parameters

D_0	δ_0	Nm	ξ	n	v_A	z_h
$[cm^2 \cdot s^{-1}]$					$[km \cdot s^{-1}]$	$[kpc]$
4.66	0.54	0.62	0.1	4	6	5

When the propagation parameters are fixed, we further study injection parameters as well as local source's age and distance. The MultiNest package is applied to perform the Bayesian inference of the corresponding parameters to obtain their posterior distributions and correlations between them allowed by the observations. The background and local source parameter set is $\Theta = \{A^P, \gamma^P, A^{\text{He}}, \gamma^{\text{He}}, q_0^P, \alpha_P, q_0^{\text{He}}, \alpha_{\text{He}}, \mathcal{R}_c, r, t, gl, gb\}$. $A^P/\text{He}, \gamma^P/\text{He}$ are the normalization and power index of background proton/helium flux, and $q_0^{P/\text{He}}, \alpha^{P/\text{He}}$ are the local protons/heliums at 1 GV and the power index. \mathcal{R}_c is the cut-off rigidity of local CRs. r, t, gl and gb denotes the local source's distance, age, longitude and latitude.

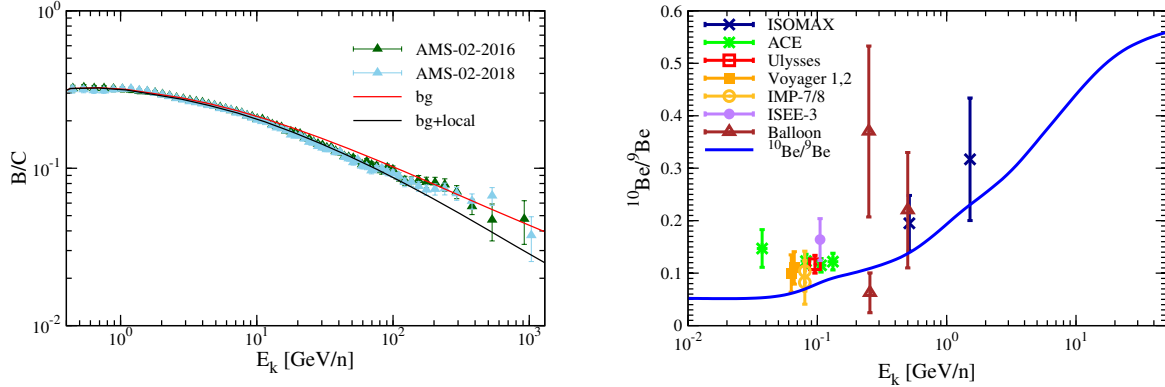


Fig. 1. Fit of the B/C and $^{10}\text{Be}/^9\text{Be}$ ratios to obtain the values of the SDP propagation parameters. The B/C data are taken from AMS-02 (Aguilar et al. 2016, 2018), and $^{10}\text{Be}/^9\text{Be}$ data are taken from ACE (Yanasak et al. (2008)), Balloon (Hagen et al. (1977), Buffington et al. (1978), Webber & Kish (1979)), ISOMAX (Hams et al. (2004)), Ulysses (Connell (1998)), ISEE-3 (Simpson & Garcia-Munoz (1988)), IMP7/8 (Garcia-Munoz et al. (1981)), Voyager (Lukasiak (1999)), respectively.

tude and latitude in the Galactic coordinate system. The data include proton and helium spectra, and the dipole anisotropy amplitude. Subject to the large systematic uncertainties of the ground-based experiments and inconsistencies in measurements, we just consider the dipole anisotropy data of AS γ and ARGO experiments for the fitting.

The 2-dimensional correlation distributions of parameters are illustrated in the triangular plot of Fig. 2. We also show the marginalized posterior PDFs in the diagonal regions. The dark, intermediate and light blue lines correspond to $1-\sigma$, $2-\sigma$ and $3-\sigma$ contours respectively. The posterior distributions of each parameter are listed in table 2. For the background parameters, A^P and γ_P (or A^{He} , γ_{He}) are distinctly anti-correlated. This can be understood that since the injection spectrum is softer, the calculated flux at normalization energy 100 GeV is lower and a larger normalization flux is needed in order to fit the spectrum. So do q_0^P and α_P (or q_0^{He} and α_{He}) of the local source.

Meanwhile as can be noticed that the age and distance of the local source has strong positive correlation. For a distant local source, its age is necessary to be old due to the longer propagation distance. Otherwise, the CRs have not propagated to the solar system so far if the source is too young. Correspondingly, its injection power has to be enhanced when its distance is far away. Therefore, q_0^P and q_0^{He} are positively correlated with source's distance r .

we also found that to explain the proton and helium spectra, the injection power index of the local source is slightly harder than the background. For example, the power index of local protons α is between -2.2 and -2.0 , whereas it is between -2.40 and -2.37 for the background. So does for helium. This has been noticed

in our previous works. Furthermore, to fit both energy spectra and anisotropy amplitude, the constraint of local source's cutoff rigidity is very tight, which is between 20 and 28 TeV. It seems to have no significantly correlations with other parameters, even does not change with local source's age and distance.

Tab. 2. Fitted injection parameters of the background and local sources

Parameter		68% limits
Background	γ^P	-2.382 ± 0.013
	$A^{P\dagger}$	0.0342 ± 0.0029
	γ^{He}	-2.311 ± 0.013
	A^{He}	0.0371 ± 0.0021
Local source	α^P	2.080 ± 0.066
	$\log_{10}(q_0^P)$	$52.57^{+0.36}_{-0.28}$
	α^{He}	2.073 ± 0.066
	$\log_{10}(q_0^{\text{He}})$	$52.15^{+0.40}_{-0.32}$
	R_c [TV]	$23.6^{+2.1}_{-2.6}$
	r [kpc]	$0.366^{+0.090}_{-0.063}$
	t [kyr]	390^{+70}_{-60}
	gl [°]	178 ± 50
	gb [°]	-19 ± 11
χ^2/dof		158.6/86

† unit of normalization $A^{P/\text{He}}$ and $q_0^{P/\text{He}}$ are $\text{GeV}^{-1} \text{m}^{-1} \text{s}^{-1} \text{sr}^{-1}$ and $\text{GeV}^{-1} \text{s}^{-1}$ respectively.

Fig. 3 shows the calculated proton and helium spectra with best-fit parameters. And Fig. 4 illustrate the corresponding amplitude and phase of anisotropy. As can be seen that, the transition from local-source dominated to background dominated in the amplitude map is a little over 100 TeV. This is due to large measurement uncer-

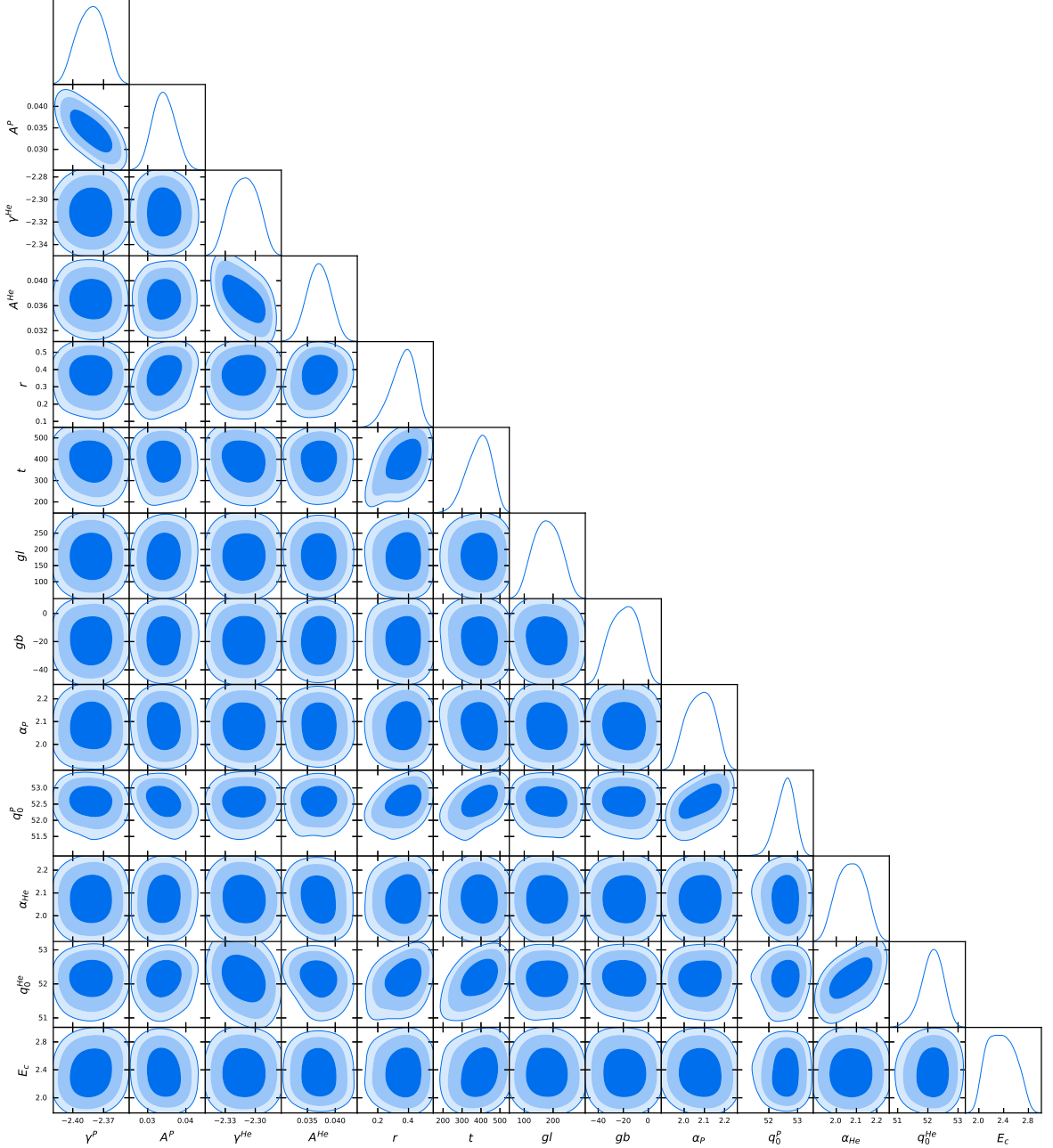


Fig. 2. 2-dimensional correlation distributions of injection parameters as well as local source's age and distance.

tainties of ARGO-2018 at that energy, so that the transition does not exactly match with AS γ data at ~ 100 TeV. We hope future experiments could make precise measurements of that transition.

Since we do not consider the phase of anisotropy, the calculated phase does not conform with observations less than 100 TeV. And thus the source's position, i.e. gb and gl , are poorly constrained, as can be seen in the Fig. 2. Above that energy, the CRs are dominated by

the background and the phase points toward Galactic center, which is consistent with observations.

When the local source's position and age are constrained, we further attempt to find out the best candidate in the local catalog. Fig. 5 shows 2-D contours of age and distance of local source with local SNRs and pulsars shown as green circle and blue square points. The Geminga pulsar, J1741-2054 and J1057-5226 are shown as red, green and yellow squares. Besides we also

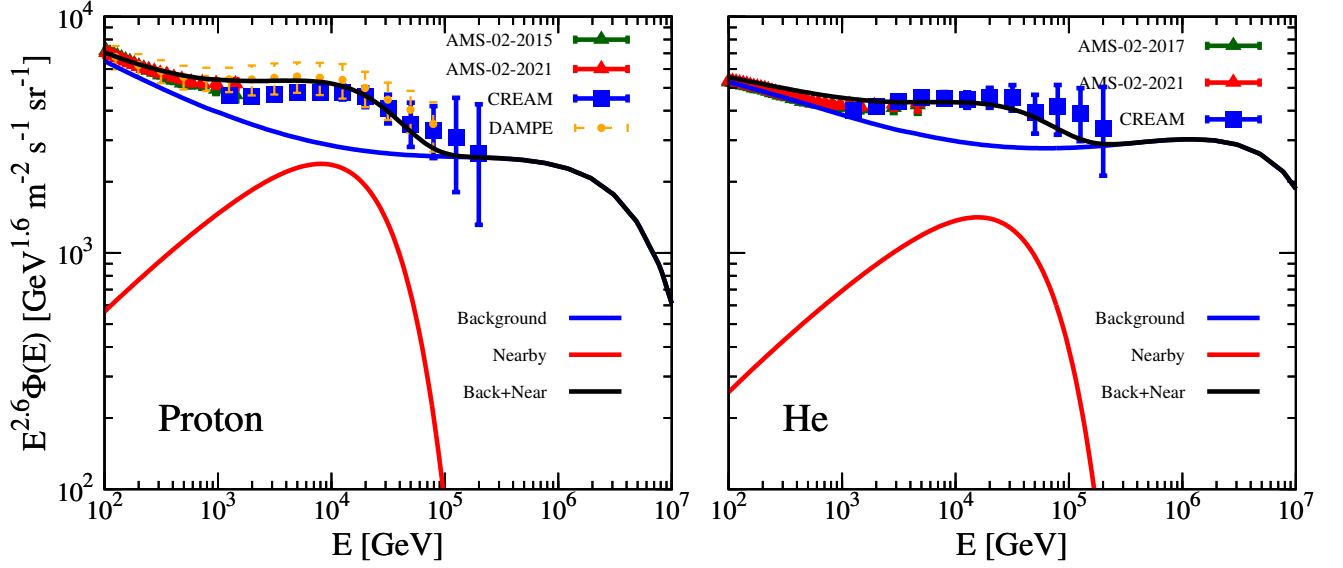


Fig. 3. Proton and helium spectra calculated with best-fit parameters. The data points are taken from AMS-02(Aguilar et al. (2015b, 2017); Aguilar et al. (2021)), CREAM(Yoon et al. (2017)), and DAMPE(An et al. (2019)).

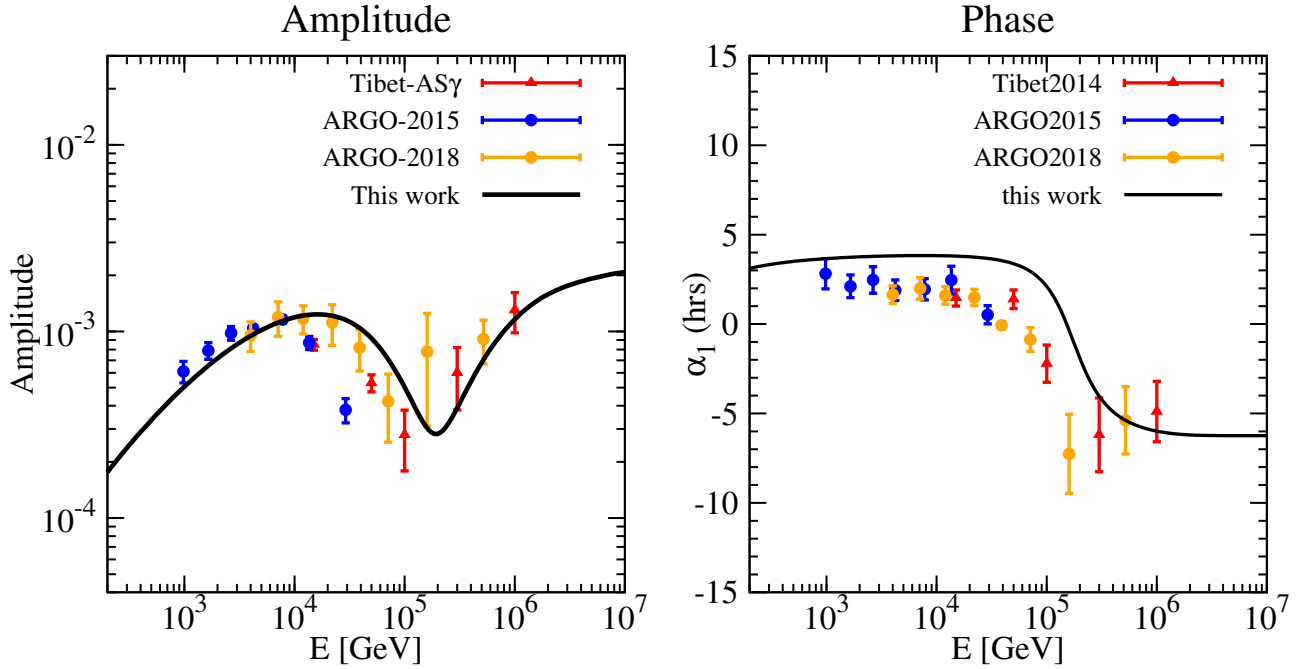


Fig. 4. Amplitude and phase of anisotropy calculated with best-fit parameters. The data points are taken from ARGO-YBJ(Bartoli et al. (2015), Bartoli et al. (2018)), Tibet(Amenomori et al. (2017)).

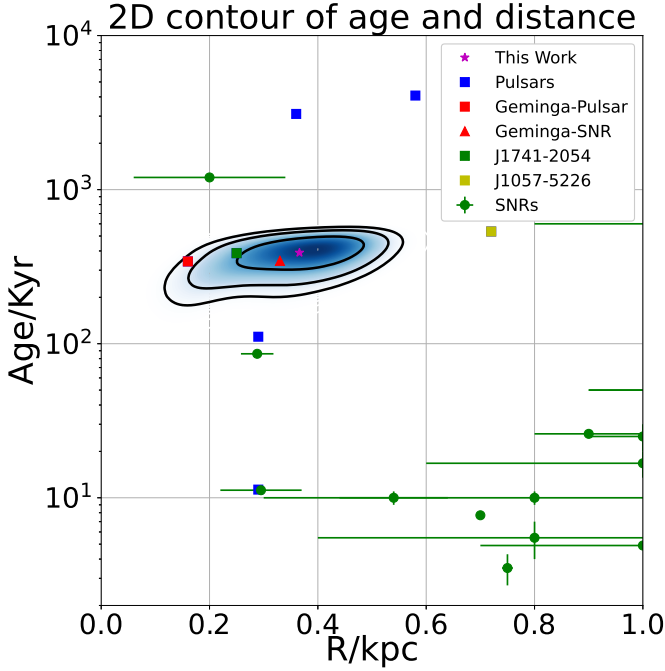


Fig. 5. 2D contour of age and distance of local source. The violet star is best fit values of galactic longitude and latitude, and the solid lines are $1-\sigma$, $2-\sigma$ and $3-\sigma$ contours respectively.

include Geminga SNR, which is taken as the local source to explain both energy spectra and anisotropy in our previous works. The violet star is best fit values of age and distance, and the solid lines are $1-\sigma$, $2-\sigma$ and $3-\sigma$ contours respectively. As can be seen from the figure, most of local sources are far from the contours and thus excluded. Only Geminga-pulsar/SNR and J1741-2054 are within the $3-\sigma$ regions. The Geminga-pulsar is just at $3-\sigma$ contour and Geminga-SNR are closest to the best-fit value.

Fig. 6 shows 2-D contour of galactic longitude and latitude. Due to lack of fitting phase of anisotropy, the permissible range of gl is quite large. Nevertheless, we can find that the constraints are still very tight and the allowed sources are only Geminga SNR and Geminga pulsar. The local sources at anti-Galactic center direction are very few, most of them are at the direction of Galactic center. And Geminga SNR is very close to the best-fit value. Therefore we think Geminga SNR is likewise the probable candidate of the local source.

4. CONCLUSION

We have built up an unified scenario, based on SDP+local source, to explain the observations of both energy spectra and anisotropy of CR nuclei below PeV energies. We find that less than ~ 100 TeV, not only does the local source contribute to the spectral hard-

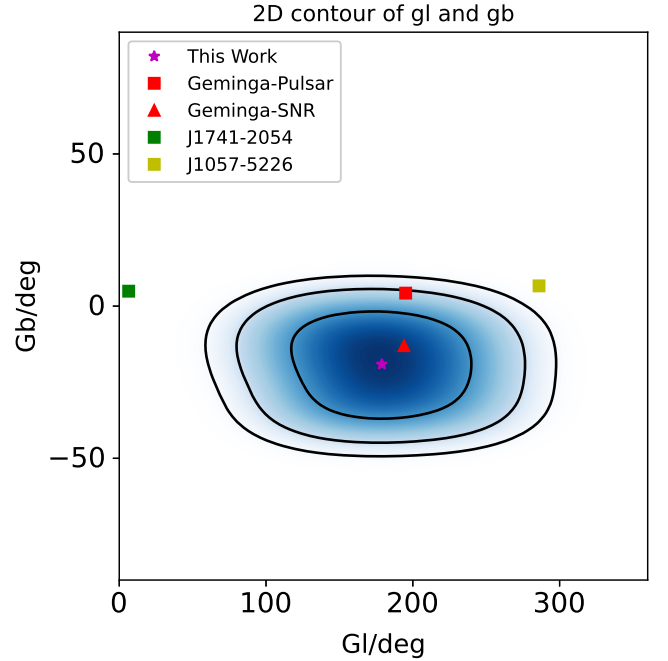


Fig. 6. 2D contour of galactic longitude and latitude. The violet star is best fit values of galactic longitude and latitude, and the solid lines are $1-\sigma$, $2-\sigma$ and $3-\sigma$ contours respectively.

enging at ~ 200 GV and subsequent softening at 20 TeV in the energy spectra, but also dominates the GCR streaming and determines the low energy anisotropy pattern. From the phase of the dipole anisotropy, we infer that the SNR associated with Geminga may be an important candidate source.

In this work, we further investigate the injection parameters and local source's position and age in detail by the aid of the Bayesian inference tool, MULTINEST. We find that the age and distance of the local source are positively correlated. For a distant local source, its age has to be older. Otherwise, the CRs could not propagate to the solar system currently if the source is too young. And the corresponding injection power is enhanced, so q_0^P and q_0^{He} are also expected to be positively correlated with source's distance r . Meanwhile both energy spectra and anisotropy amplitude severely constrain the local source's cutoff rigidity, which is between 20 and 28 TV.

The energy spectra and anisotropy amplitude also give strong constraints of local source age and distance to the solar system. Most of local sources have been excluded and we find that only Geminga SNR is very close to the best-fit value. In addition, despite that the permissible range of gl and gb is quite large, most of local sources are also excluded, since most of them are in the direction of

Galactic center. Only Geminga SNR is very close to the best-fit value. From these, we infer that the Geminga SNR could be the probable candidate of local source.

Since the Geminga SNR is still away from the direction of observation phase, we do not include the amplitude of anisotropy into fitting. In the future work, we would take the influence of local ordered magnetic field into account to better reproduce the observational phase less than 100 TeV. And based on the reproduced phase, we would like to find out the candidate of CR nuclei source from the local catalog.

ACKNOWLEDGEMENTS

This work is supported by the National Key Research and Development Program of China (No. 2018YFA0404202), the National Natural Science Foundation of China (Nos. 11635011, 11875264, U1738209, U2031101, U2031110).

Software: DRAGON (Evoli et al. (2008, 2017)) available at <https://github.com/cosmicrays>.

MULTINEST (Feroz & Hobson (2008); Feroz et al. (2009)) available at <https://github.com/farhanferoz/MultiNest>.

REFERENCES

- Abdo, A. A., Ackermann, M., Ajello, M., et al. 2009, *Physical Review Letters*, 102, 181101
- Abeysekara, A. U., Albert, A., Alfaro, R., et al. 2017, *Science*, 358, 911
- Accardo, L., Aguilar, M., Aisa, D., et al. 2014, *Physical Review Letters*, 113, 121101
- Adriani, O., Barbarino, G. C., Bazilevskaya, G. A., et al. 2009, *Nature*, 458, 607
- . 2011, *Science*, 332, 69
- Adriani, O., Akaike, Y., Asano, K., et al. 2019, *Phys. Rev. Lett.*, 122, 181102
- Aguilar, M., Aisa, D., Alvino, A., et al. 2014, *Physical Review Letters*, 113, 121102
- Aguilar, M., Aisa, D., Alpat, B., et al. 2015a, *Physical Review Letters*, 115, 211101
- . 2015b, *Physical Review Letters*, 114, 171103
- Aguilar, M., Ali Cavasonza, L., Ambrosi, G., et al. 2016, *Phys. Rev. Lett.*, 117, 231102
- Aguilar, M., Ali Cavasonza, L., Alpat, B., et al. 2017, *Physical Review Letters*, 119, 251101
- Aguilar, M., Ali Cavasonza, L., Ambrosi, G., et al. 2018, *Phys. Rev. Lett.*, 120, 021101
- Aguilar, M., Ali Cavasonza, L., Ambrosi, G., et al. 2021, *Physics Reports*, 894, 1, the Alpha Magnetic Spectrometer (AMS) on the International Space Station: Part II - Results from the First Seven Years
- Aharonian, F., Akhperjanian, A. G., Anton, G., et al. 2009, *A&A*, 508, 561
- Ahlers, M. 2016, *Phys. Rev. Lett.*, 117, 151103
- Amenomori, M., Bi, X. J., Chen, D., et al. 2017, *ApJ*, 836, 153
- An, Q., Asfandiyarov, R., Azzarello, P., et al. 2019, *Science Advances*, 5, eaax3793
- Atkin, E., Bulatov, V., Dorokhov, V., et al. 2017, *J. Cosmology Astropart. Phys.*, 7, 020
- Baade, W., & Zwicky, F. 1934, *Contributions from the Mount Wilson Observatory*, 3, 79
- Bartoli, B., Bernardini, P., Bi, X. J., et al. 2015, *ApJ*, 809, 90
- Bartoli, B., Bernardini, P., Bi, X. J., et al. 2018, *The Astrophysical Journal*, 861, 93
- Bernard, G., Delahaye, T., Salati, P., & Taillet, R. 2012, *A&A*, 544, A92
- Blasi, P., & Amato, E. 2012, *J. Cosmology Astropart. Phys.*, 1, 11
- Borla Tridon, D. 2011, *International Cosmic Ray Conference*, 6, 47
- Buffington, A., Orth, C. D., & Mast, T. S. 1978, *ApJ*, 226, 355
- Cardillo, M., Tavani, M., & Giuliani, A. 2014, *Nuclear Physics B Proceedings Supplements*, 256, 65
- Connell, J. J. 1998, *ApJ*, 501, L59
- DAMPE Collaboration, Ambrosi, G., An, Q., et al. 2017, *Nature*, 552, 63
- Dubner, G., & Giacani, E. 2015, *A&A Rev.*, 23, 3
- Erlykin, A. D., & Wolfendale, A. W. 1997, *Journal of Physics G Nuclear Physics*, 23, 979
- Evoli, C., Gaggero, D., Grasso, D., & Maccione, L. 2008, *J. Cosmology Astropart. Phys.*, 10, 018
- Evoli, C., Gaggero, D., Vittino, A., et al. 2017, *J. Cosmology Astropart. Phys.*, 2, 015
- Fang, K., Bi, X.-J., Yin, P.-F., & Yuan, Q. 2018, *ApJ*, 863, 30
- Feng, J., Tomassetti, N., & Oliva, A. 2016, *Phys. Rev. D*, 94, 123007
- Feroz, F., & Hobson, M. P. 2008, *MNRAS*, 384, 449
- Feroz, F., Hobson, M. P., & Bridges, M. 2009, *MNRAS*, 398, 1601
- Feroz, F., Hobson, M. P., Cameron, E., & Pettitt, A. N. 2019, *The Open Journal of Astrophysics*, 2, 10
- Funk, S. 2015, *Annual Review of Nuclear and Particle Science*, 65, 245

- Garcia-Munoz, M., Simpson, J. A., & Wefel, J. P. 1981, in International Cosmic Ray Conference, Vol. 2, International Cosmic Ray Conference, 72
- Gleeson, L. J., & Axford, W. I. 1968, *ApJ*, 154, 1011
- Green, D. A. 2015, *MNRAS*, 454, 1517
- Guo, Y.-Q., Tian, Z., & Jin, C. 2016, *ApJ*, 819, 54
- Guo, Y.-Q., & Yuan, Q. 2018, *Phys. Rev. D*, 97, 063008
- Hagen, F. A., Fisher, A. J., & Ormes, J. F. 1977, *ApJ*, 212, 262
- Hams, T., Barbier, L. M., Bremerich, M., et al. 2004, *ApJ*, 611, 892
- Hewitt, J. W., & Lemoine-Goumard, M. 2015, *Comptes Rendus Physique*, 16, 674
- Liu, W., Bi, X.-J., Lin, S.-J., Wang, B.-B., & Yin, P.-F. 2017, *Phys. Rev. D*, 96, 023006
- Liu, W., Guo, Y.-Q., & Yuan, Q. 2019, *J. Cosmology Astropart. Phys.*, 2019, 010
- Liu, W., Yao, Y.-h., & Guo, Y.-Q. 2018, *ApJ*, 869, 176
- Lukasiak, A. 1999, International Cosmic Ray Conference, 3, 41
- Mertsch, P. 2011, *J. Cosmology Astropart. Phys.*, 2, 31
- Panov, A. D., Adams, J. H., J., Ahn, H. S., et al. 2007, *Bulletin of the Russian Academy of Sciences, Physics*, 71, 494
- Panov, A. D., Adams, J. H., Ahn, H. S., et al. 2009, *Bulletin of the Russian Academy of Sciences, Physics*, 73, 564
- Perko, J. S. 1987, *A&A*, 184, 119
- Putze, A., Derome, L., Maurin, D., Perotto, L., & Taillet, R. 2009, *A&A*, 497, 991
- Qiao, B.-Q., Liu, W., Guo, Y.-Q., & Yuan, Q. 2019, *J. Cosmology Astropart. Phys.*, 2019, 007
- Simpson, J. A., & Garcia-Munoz, M. 1988, *Space Sci. Rev.*, 46, 205
- Skilling, J. 2004, in American Institute of Physics Conference Series, Vol. 735, *Bayesian Inference and Maximum Entropy Methods in Science and Engineering: 24th International Workshop on Bayesian Inference and Maximum Entropy Methods in Science and Engineering*, ed. R. Fischer, R. Preuss, & U. V. Toussaint, 395–405
- Staszak, D., Abeysekara, A. U., Archambault, S., et al. 2015, *ArXiv e-prints*, arXiv:1510.01269
- Tang, X., & Piran, T. 2019, *MNRAS*, 484, 3491
- Tian, Z., Liu, W., Yang, B., et al. 2020, *Chinese Physics C*, 44, 085102
- Tomassetti, N. 2012, *ApJ*, 752, L13
- . 2015, *Phys. Rev. D*, 92, 081301
- Trotta, R. 2008, *Contemporary Physics*, 49, 71
- Trotta, R., Jóhannesson, G., Moskalenko, I. V., et al. 2011, *ApJ*, 729, 106
- Webber, W. R., & Kish, J. 1979, in International Cosmic Ray Conference, Vol. 1, International Cosmic Ray Conference, 389
- Yanasak, N., Wiedenbeck, M., Mewaldt, R., et al. 2008, *The Astrophysical Journal*, 563, 768
- Yoon, Y. S., Ahn, H. S., Allison, P. S., et al. 2011, *ApJ*, 728, 122
- Yoon, Y. S., Anderson, T., Barrau, A., et al. 2017, *ApJ*, 839, 5
- Yuan, Q., Qiao, B.-Q., Guo, Y.-Q., Fan, Y.-Z., & Bi, X.-J. 2020, *arXiv e-prints*, arXiv:2007.01768